Available on CMS information server **CMS AN -2009/164**

The Compact Muon Solenoid Experiment

Analysis Note

The content of this note is intended for CMS internal use and distribution only

05 November 2009 (v4, 06 January 2010)

Electron Reconstruction in CMS

W. Adam [a)], S. Baffioni [b)], F. Beaudette [c)], D. Benedetti [c)], C. Broutin [b)], D. Chamont [b)], C. Charlot [b)], E. DiMarco [d)], D. Futyan [e)], S. Harper [f)], D. Lelas [g)], A. Martelli [h)], P. Meridiani [c)], M. Pioppi [e)], I. Puljak [g)], D. Sabes [b)], R. Salerno [h)], M. Sani [i)], C. Seez [e)], Y. Sirois [b)], P. Vanlaer [j)], D. Wardrope [e)]

Abstract

The CMS electron reconstruction algorithms and expected performance from a detailed Monte Carlo simulation are presented. The energy deposited in the electromagnetic calorimeter is measured in clusters of clusters (superclusters) which collect bremsstrahlung photons emitted in the tracker volume. Electron tracks are seeded using the innermost tracker layers. The ECAL driven seeding algorithm, optimised for isolated electrons in the p_T range relevant for Z or W decays and down to $p_T \simeq 5$ GeV/c, is complemented by a tracker driven seeding more suitable for low p_T electrons and/or electrons inside jets. Trajectories are reconstructed using a dedicated modeling of the electron energy loss and fitted with a Gaussian Sum Filter. Electron candidates are preselected using loose cuts on track-cluster matching observables so to preserve the highest possible efficiency while removing part of the QCD background. A cleaning is performed to resolve cases where several tracks are reconstructed from the conversion legs of radiated photons. The electron charge is determined by comparing different charge measurement observables to better cope with the mis-identification that arises from early conversions of radiated photons. Electrons are classified using observables sensitive to the pattern of bremsstrahlung emission and showering in the tracker material. The electron energy is deduced from a weighted combination of the supercluster energy and tracker momentum measurements based on the electron classes. The electron direction is that of the reconstructed electron track at the interaction point. The specific algorithms developed for the cases of low p_T electrons and non-isolated electrons are presented. Finally, possible effects of startup conditions of the LHC are discussed.

a) HEPHY, Institut für Hochenergiephysik der OeAW, Vienna

b) LLR, Laboratoire Leprince-Ringuet, Ecole Polytechnique, IN2P3-CNRS, Palaiseau

c) CERN, European Organisation for Nuclear Research, Geneva

d) Università di Roma ”La Sapienza”, INFN, Roma

e) Imperial College, University of London, London

f) RAL, Rutherford Appleton laboratory, Didcot

g) FESB, Technical University of Split, Split

h) Università di Milano-Bicocca, INFN, Milano

i) UCSD, University of California, San Diego

j) Université Libre de Bruxelles, Bruxelles

the electron classes. The electron direction is that of the reconstructed electron track at the interaction point. The specific algorithms developed for the cases of low p_T electrons and non-isolated electrons are presented. Finally, possible effects of startup conditions of the LHC are discussed.

1 Introduction

Initial algorithms for electron reconstruction were developed in the context of the online selection in the HLT for the DAQ TDR [1, 2]. The main strategy for the offline reconstruction of electrons in CMS was established for the Physics Technical Design Report [3, 4] and optimised in particular on the H $\rightarrow$ ZZ*$\rightarrow$ e$^+$e$^-$e$^+$e$^-$ benchmark channel [5]. It starts by the reconstruction of superclusters in the ECAL that are built from elementary clusters to collect the energy lost by bremsstrahlung radiation in the tracker material and spread in ϕ by the strong solenoidal magnetic field. A dedicated tracking is used based on the "Gaussian Sum Filter" (GSF) fit procedure [6, 7] which relies on a proper modeling of electron radiative energy loss. This procedure allows for an efficient collection of hits up to the ECAL and a measurement of the true fraction of emitted bremsstrahlung by the comparison of the outermost and innermost track momentum estimates [8]. This measurement, as well as in general track estimates at the outermost position, have proven to be useful ingredients of electron identification algorithms [8, 9, 10, 11]. The electron momentum is estimated by combining the tracker and ECAL measurements [12]. In this procedure, electron classes allow to separate electrons whose energy measurement suffered much from bremsstrahlung losses from those having undergone little radiation emission, by exploiting information from the observed cluster pattern, the tracker estimate of the fraction of emitted bremsstrahlung, and the ratio E/p. This allows to better cope with the non gaussian fluctuations induced on both the ECAL and tracker measurements by the presence of material in the tracker.

Since the Physics TDR, the description of the tracker material has become more realistic leading to an overal budget peaking at $\simeq 2X_0$ for a pseudorapidity $|\eta| \simeq 1.5$. As a consequence, the effect of subsequent conversions of radiated photons and in general more complicated showering of the electrons have lead to more pronounced effects in the reconstruction with in particular a high rate of charge mis-identification and the need for more elaborated conversion removal. On the other hand, important progress has been made on the reconstruction efficiency, in particular in the low p_T region, by a retuning of the ϕ windows used at the different steps of the reconstruction and by the additional use of a tracker driven seeding algorithm [13]. The algorithms developed for the reconstruction of non-isolated electrons are now used together with those optimized for the isolated case, so that all electron candidates are provided in a single collection.

This note describes the current status of algorithms for electron reconstruction in CMS. It complements previous work and documents the performance of the reconstruction based on full Monte Carlo simulation prior to first collision data. The presented performance have been obtained using CMSSW version 3 [1)]. Samples of back-to-back electrons with uniform transverse momentum p_T^e distribution from 2 to 150 GeV/c and uniform η^e distribution, as well as with the kinematics of Z$\rightarrow$e$^+$e$^-$ decays are used to illustrate the performance in the isolated case. For the background, samples of QCD di-jet events in different p_T^{hat} bins ranging from 0 to 300 GeV/c are used. Electrons from b-jets with p_T^{hat} within 20-120 GeV/c are used for the non-isolated case. Finally, a sample of back-to-back electrons with a uniform p_T distribution between 2 and 10 GeV/c is used for the evaluation of the performance at lowest p_T^e.

2 Electron Seeding

The reconstruction of electrons in CMS starts by the reconstruction of clusters seeded by hot cells in the ECAL, which are used to form superclusters to further collect the energy radiated by bremsstrahlung in the tracker volume. The hybrid algorithm [2] is used in the barrel, with superclusters obtained by grouping dominoes within a ϕ window around the starting crystal up to a maximum extension of 0.3 rad in both directions. In the ECAL endcaps, the "multi5x5" algorithm is used. It first collects the energy deposited in the crystals within 5$\times$5 matrices and superclusters are then formed by grouping such clusters whose position lies within a ϕ road of extension 0.3 rad in ϕ, as for the barrel case.

Following [1, 14], the superclusters are then used to select trajectory seeds built from the combination of hits from the innermost tracker layers. Superclusters are first preselected using a hadronic veto cut and applying a 4 GeV threshold on the supercluster transverse energy. The hadronic veto is defined by the ratio H/E of the hadronic energy as estimated by summing HCAL towers energy within a cone of $\Delta R = 0.15$ behind the supercluster position over the supercluster energy. Figure 1 shows the efficiency/rejection curves as obtained from this variable for a an electron passing all other pre-selection cuts. Contributions are shown separately for electrons in the ECAL barrel ($|\eta_{SC}| < 1.442$), in the ECAL endcaps ($1.56 < |\eta_{SC}| < 2.5$) and in the barrel-endcap transition

[1)] Samples are from CMSSW 312 from the official summer 09 or private productions and have been reprocessed wherever appropriate so to include electron algorithms version consistent with what is included in CMSSW 340 regions ($1.442 < |\eta_{SC}| < 1.56$). Electrons are from Z→ee decays for the signal and from QCD di-jet events and p_T^{hat} within 15-170 GeV/c for the background. A cut value of 0.15 is used. After applying the preselection cuts described in 4, it corresponds to an electron (resp. jet) efficiency of 98.8% (resp. 54.5%) overall, and of 99.3% (resp. 58.8%) in the ECAL barrel, 99.2% (resp. 48.6%) in the ECAL endcaps and 85% (resp. 53%) in the transition region between the barrel and endcap parts. The efficiency of this cut as a function of the generated electron p_T^e is also shown on Fig. 1.

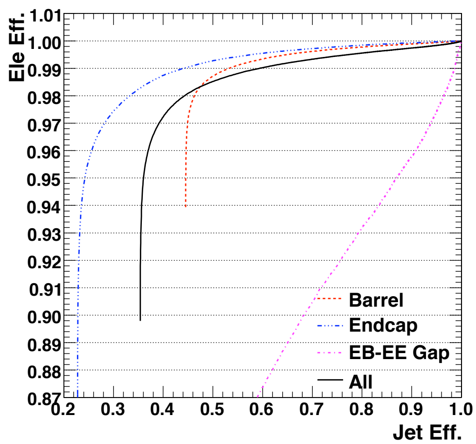

(a)

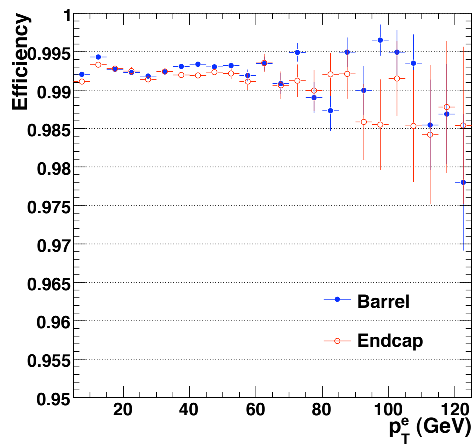

(b)

Figure 1: Performance of the H/E observable for the ecal driven seeding: (a) efficiency/rejection curves for all electrons (solid line, black), for electrons in the ECAL barrel (dashed, red), in the ECAL endcaps (dashed-dotted-dotted, blue) and in the transition region between barrel and endcaps (dashed-dotted, magenta); (b) efficiency as a function of the generated electron p_T^e. Electrons are from a sample of Z→ee decays for the signal and from a sample of QCD di-jet events with p_T^{hat} = 15-170 GeV/c for the background. The preselection cuts described in Sec. 4 have been applied.

The seeding algorithm combines pixel and TEC layers so to gain in efficiency in the forward region where the coverage by the forward pixel layers is limited. The selection is made by matching the superclusters with trajectory seeds build from hit pairs or triplets. Windows in ϕ and z (or transverse radius r_T in the forward region) are used to match the 2 hits of each trajectory seeds, taking into account both charge hypotheses. In case of triplets, at least two out of the three hits are required to be matched. This procedure takes advantage of the fact that the supercluster position is on the helix of the initial electron trajectory, so that one can predict the position of the hits backpropagating the helix parameters through the magnetic field toward the innermost part of the measured trajectory, before which radiation is unlikely to have occured. This strategy, developed for HLT, allows for an efficient filtering of background from jets faking electrons. The first layer windows are made loose in both ϕ and z (or r_T) in order to account for residual material effects and for the beam spot position uncertainty σ_z along the z axis. Once a hit is matched on the first layer, this information is used to refine the helix parameters and a second hit is looked for in the second layer using smaller windows. In order to further reduce the contamination from fake electrons from jets, the first ϕ window is made E_T dependent, where E_T is the measured transverse energy from the supercluster. The matching windows have been recently reoptimised [15] and their definitions are presented in Table. 1.

	1st windows		2nd windows			
	δz or δr_T	$\delta\phi$	δz	δr_T (PXF)	δr_T (TEC)	$\delta\phi$
10 GeV/c	$\pm 5\sigma_z$	[-0.14;0.08] rad	$\pm$0.09 cm	$\pm$0.15 cm	$\pm$0.2 cm	$\pm$4 mrad
35 GeV/c	$\pm 5\sigma_z$	[-0.05;0.03] rad	$\pm$0.09 cm	$\pm$0.15 cm	$\pm$0.2 cm	$\pm$4 mrad

Table 1: Definition of the seed matching windows. The E_T-dependent first ϕ window extension is given for 10 and 35 GeV/c. σ_z is the beam spot width along the z axis.

This ECAL driven electron seeding strategy is very efficient for isolated electrons with $p_T^e \gtrsim 10$ GeV$/c$. At lower p_T^e, the ϕ window used for the superclusters starts to be too small and some electrons which radiates leads to electron and photon clusters more separated than 0.3 rad in the magnetic field. Moreover, for the cases of electrons in jets, the energy collected in the superclusters may include some neutral contribution from the jets therefore biasing the energy measurement used to seed electron tracks. For these reasons, the above seeding strategy is complemented by a tracker driven algorithm, developed in the context of the particle-flow event reconstruction [17]. The tracker driven seeding starts from the high purity tracks, and makes use of the particle flow clustering which exploits the fine ECAL granularity.

The tracker driven seeding algorithm, described in details in [13], can be illustrated with two extreme cases. When an electron does not radiate energy by bremsstrahlung while traversing the tracker, it gives rise to a single cluster in the ECAL and its track is often well reconstructed by the standard (MIP) Kalman Filter which is able in these cases to collect hits up to the ECAL entrance. The track can then be matched with a particle flow cluster, and its momentum compared to the cluster energy forming an E/p ratio. If this ratio is close to unity, the seed of the track is promoted to electron seed. Alternatively, when an electron undergoes a significant bremsstrahlung, the standard Kalman Filter is not able to follow the change of curvature, and the track has a small number of hits, and a large χ^2. Thus, using the tracker as a preshower, and exploiting the differences of characteristics between a pion track and an electron track reconstructed with the standard Kalman Filter algorithm, the electron tracks can be selected. The variety of situations between the two extreme cases illustrated here requires a treatment more sophisticated than what was just described. In practice, a refined treatment of the track is applied, and the pure tracking observables are combined with the ECAL-track matching quality variables in a single discriminator with a multivariate analysis.

Seeds from the two algorithms are then merged in a single collection, keeping track of the seed provenance. Figure 2 shows the resulting seeding efficiency as a function of generated electron η^e and p_T^e for electrons from a sample of Z→ee decays. The separate contribution of each algorithm is also shown.

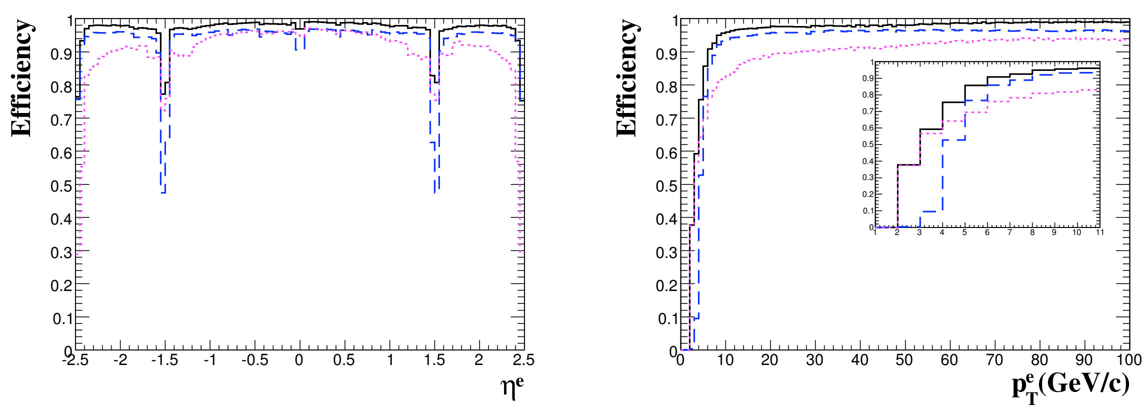

(a) (b)

Figure 2: Electron seeding efficiency (solid line) as a function of (a) generated electron η^e and (b) generated electron p_T^e for a sample of electrons with uniform distibution in η^e and p_T^e and for $p_T^e > 2$ GeV$/c$. The individual contributions from the ECAL driven (dashed line) and from the tracker driven seeding algorithms are also shown, as well as a zoom of the region $p_T^e < 11$ GeV$/c$.

Although the tracker driven seeding has been primarily developed and optimised for non isolated electrons, it brings additional efficiency on isolated electrons, in particular in the ECAL crack regions ($\eta \simeq 0$ and $|\eta| \simeq 1.5$) and, as expected, at low p_T^e. At 5 GeV$/c$, the seeding efficiency is increased by 12.5% by combining with tracker driven seeds. Below this value, the seeding efficiency is entirely dominated by the tracker driven seeds and at high p_T^e, the additional efficiency brought by the tracker driven approach is at the 1-2% level.

The seeding performance have been also evaluated for the case of non isolated electrons. Figure 3 presents the seeding efficiency for electrons and pions with $p_T^e > 2$ GeV$/c$ as a function of η^e and p_T^e on a sample of electrons from b-jets with p_T^{hat} within 20-120 GeV$/c$. As can be expected, the seeding efficiency for non-isolated electrons is much improved by the tracker driven seeding. Overall, an efficiency of 77% for electrons and 10.5% for pions is obtained.

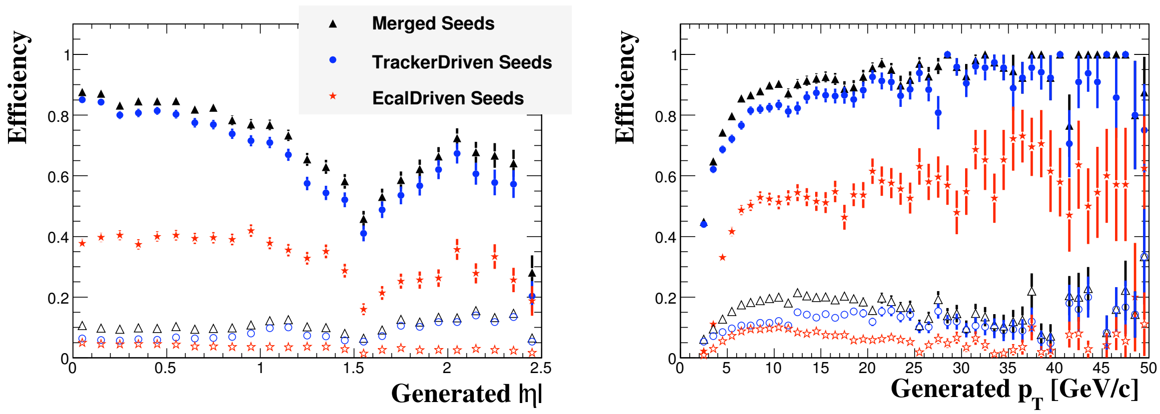

(a) (b)

Figure 3: Seeding performance for non-isolated electrons from a sample of b-jets with p_T^{hat} within 20-120 GeV$/c$ as a function of (a) generated $|\eta^e|$ and (b) generated p_T^e; efficiencies are shown for electrons (plain markers) and pions (empty markers) as well as separately for the ECAL driven seeding (stars), the tracker driven seeding (circles) and after the merging of both algorithms (triangles).

3 Electron Tracking

Electron seeds are then used to initiate a dedicated electron track building and fitting procedure in order to best handle the effect of bremsstrahlung energy loss [6]. The track finding is based on a combinatorial Kalman Filter as described in [16], with a dedicated Bethe Heitler modeling of the electron energy losses. In order to preserve efficiency and to follow electron trajectories in case of bremsstrahlung emission, a very loose χ^2 compatibility is required in the building steps of the electron tracking, with a cut value of 2000. The combinatorics is limited by requiring at most 5 candidate trajectories at each tracker layer and at most one layer with a missing hit. Finally, in order to reduce the probability to connect a primary electron to a leg from a photon conversion, a high χ^2 penalty (90.) is used in the cases of missing hit.

The number of collected hits from the electron track reconstruction procedure is compared in Figure. 4 with the standard Kalman Filter used for pions and muons. The differences arise from the choices of the modeling of the energy loss and of the trajectory building parameters. The electron track reconstruction procedure allows to collect hits up to the ECAL, despite the presence of electron energy loss in the tracker material. On the contrary, the standard Kalman Filter in average leads to shorter tracks, the reconstruction of the electron trajectory being stopped when important change of curvature arises from bremsstrahlung radiation.

The hits collected in the track finding phase are passed to a GSF for the final estimation of the track parameters. In such fit, the energy loss in each layer is approximated by a weighted sum of Gaussian distributions. The GSF leads to multi-component trajectory states for each measurement point, with weights for each component describing the associated probability. Although more information is available, one usually considers two combinations in order to estimate the track momentum parameters at each measurement point: the weighted mean of the components (so called "mean") and highest weight component (so called "mode"). While the mean estimate is in average less biased, it has been shown [4] that the mode estimate is more precise for low radiating tracks. On the contrary, tracks that have been subject to important bremsstrahlung losses have their reconstructed momentum underestimated, creating a typical low momentum tail. Figure 5 shows the residual distributions of the track momentum parameters at the innermost track position for the mean and mode estimates on a sample of electrons from Z→ee decays.

Figure 6 presents the comparison between the track momentum parameters as obtained from the GSF fit and using the mode estimate with the parameters obtained using the standard Kalman Filter procedure as used for MIPs. The results are shown for electrons from a sample of Z→ee decays. One can see that the GSF mode estimate is more precise, in particular for the ϕ direction. The transverse momentum reconstruction show a less biased measurement for tracks having been subject to bremsstrahlung emission, while a similar resolution is observed from the right hand side of the distribution.

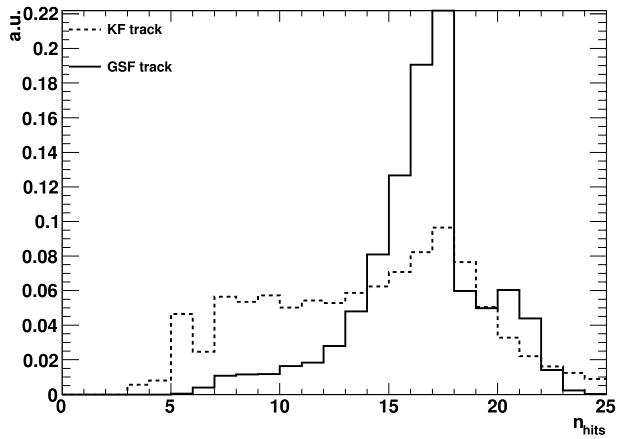

Figure 4: Number of reconstructed hits per track for electrons from Z→ee decays: distribution as obtained with the dedicated tracking procedure used for electrons (solid line) and with the standard Kalman Filter used for MIPs (dashed line).

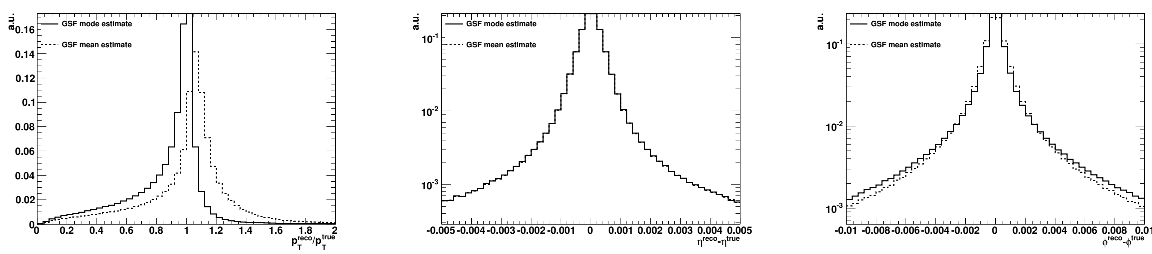

(a) (b) (c)

Figure 5: Electron track momentum parameters residual distributions for the "mode" (solid line) and the "mean" (dashed line) estimates at the innermost track position and for electrons from a sample of Z→ee decays: (a) transverse momentum magnitude (b) momentum η direction and (c) momentum ϕ direction.

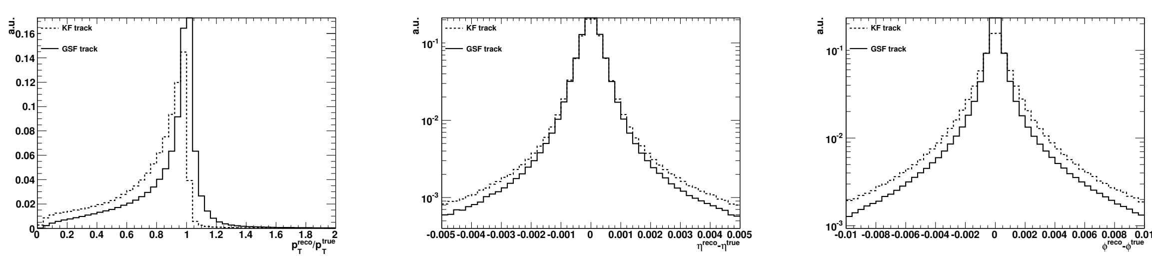

(a) (b) (c)

Figure 6: Electron track momentum parameters residual distributions for the "mode" estimates at the innermost track position for both the dedicated GSF electron tracking (solid line) and the standard Kalman Filter used for MIPs (dashed line): (a) momentum η direction (b) momentum ϕ direction and (c) transverse momentum magnitude. Electrons are from a sample of Z→ee decays.

Finally, the difference between the momentum magnitude at the outermost track position and at the innermost track position is an estimate of the true fraction of energy radiated by the electron [4]. The normalised difference called "f_{brem}" is shown on Fig. 7 for electron from Z→ee decays and for a background constituted by QCD dijet events with p_T^{hat} within 80-120 GeV/c. The distribution is nearly flat for the signal while for the background it peaks at low f_{brem} values as expected from a background constituted by charged hadrons which do not radiate. This variable is used in the electron classification that enters the final electron momentum estimation and is an important ingredient of electron identification algorithms.

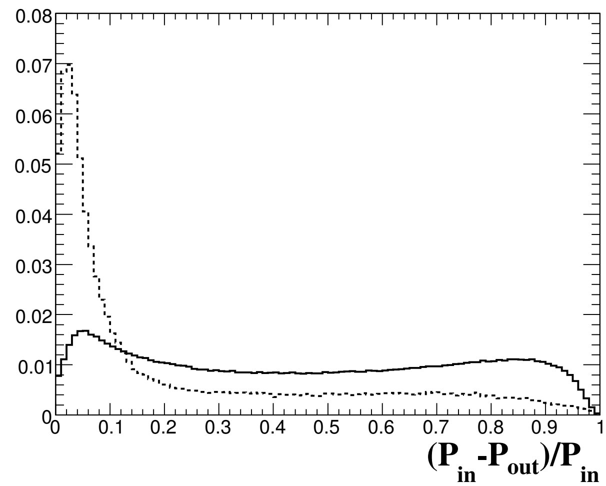

Figure 7: Electron bremsstralhung fraction f_{brem} as measured from the normalised difference between the momentum estimate at the innermost and at the outermost track positions, and for (solid line) electrons from Z→ee decays and (dashed line) background from a sample of QCD dijet events with p_T^{hat} within 80-120 GeV/c.

4 Electron Preselection

Electron candidates are built from the reconstruction of GSF tracks and their associated superclusters.

In the case of electrons with ECAL driven seeds, the associated supercluster is simply the supercluster that initiated the seed reconstruction. For the cases of electrons with seeds only found by the tracker driven seeding algorithm, a tracker driven bremsstrahlung recovery algorithm and identification of the “electron cluster” developed in the context of the particle flow reconstruction [17, 18] is used. This tracker driven algorithm runs on all GSF tracks to produce superclusters by grouping together particle flow clusters which are matched with presumed “photon” lines, tangent to the electron trajectory at any of the tracker measurement layers. The electron cluster, defined as the cluster matched with the outermost track state, is finally added to the supercluster. This procedure, whose performance are described in more details in section 8, leads to a new collection of superclusters that are used to build the electron candidates for the cases of electrons with tracker driven only seeds. In addition, several track-cluster matching observables are combined, together with the track p_T and η, using a boosted decision tree (BDT) to obtain a global identification variable hereafter called “mva”. The observables used include pure tracking observables based on the GSF track and the comparison with the track as obtained from the standard (MIP) track reconstruction, observables relative to the energy matching between the track and the calorimeter, the bremsstrahlung photon cluster pattern analysis and the cluster shape of the electron cluster. The mva, together with the supercluster built in this procedure, are made available for all GSF tracks.

Electron candidates, formed by the association of a GSF track and its associated supercluster, are then preselected using available track-cluster matching observables in order to reduce the rate of jets faking electrons. The preselection is made very loose so to efficiently reconstruct electrons and satisfy a large number of possible analyses.

For electrons that have an ECAL driven seed, the following cuts have been already applied at the seeding level:

- $E_T > 4$ GeV/c, where E_T is the supercluster transverse energy,
- $H/E < 0.15$, where H is the energy deposited in the HCAL towers in a cone of radius $\Delta R = 0.15$ centered on the electromagnetic supercluster position and E is the energy of the electromagnetic supercluster.

In addition to this selection, the following requirements are also applied on electrons with ECAL driven seeds:

- $|\Delta\eta_{\rm in}| = |\eta_{\rm sc} - \eta_{\rm in}^{\rm extrap.}| < 0.02$, where $\eta_{\rm sc}$ is the energy weighted position in η of the supercluster and $\eta_{\rm in}^{\rm extrap.}$ is the η coordinate of the position of closest approach to the supercluster position, extrapolating from the innermost track position and direction,
- $|\Delta\phi_{\rm in}| = |\phi_{\rm sc} - \phi_{\rm in}^{\rm extrap.}| < 0.15$, where $\phi_{\rm sc}$ is the energy weighted position in ϕ of the supercluster and $\phi_{\rm in}^{\rm extrap.}$ is the η coordinate of the position of closest approach to the supercluster position, extrapolating from the innermost track position and direction.

The distributions of the matching observables used in the preselection of ECAL driven electrons, as well as the E/p distribution, are shown in Fig. 8 for electrons from Z→ee decays.

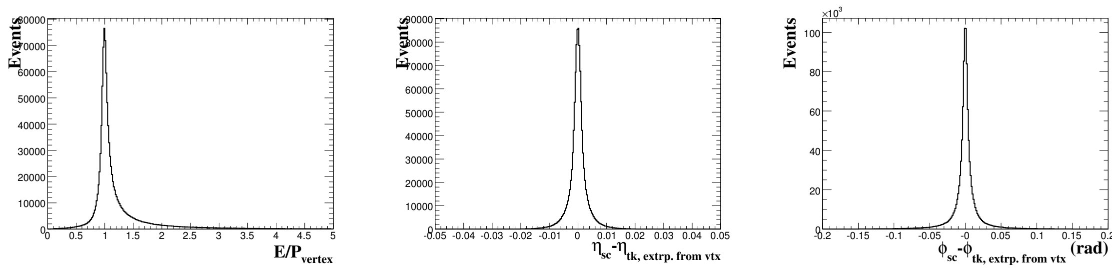

Figure 8: Electron track-cluster matching distributions for electrons from Z→ee decays (a) E/p (b) η_{SC}-η_{tk} and (c) ϕ_{SC}-ϕ_{tk}. The track positions η_{tk} and ϕ_{tk} are obtained by extrapolating from the innermost track measurement toward the supercluster position. The track momentum p is taken at the innermost track measurement.

For the cases of electrons with seed only found by the tracker driven algorithm, the global identification variable mva as obtained from the BDT is used. Electron candidates in these cases are required to satisfy:

- mva > -0.4, where mva is the output of BDT.

The distribution of the mva variable used for the preselection of electrons with tracker driven only seed is presented on Fig. 9 for electrons in b-jets and from Z→ee decays, as well as for pions in b-jets. A very good separation between electrons and pions is achieved when the electrons are isolated. The electron-pion separation remains good for electrons in jets.

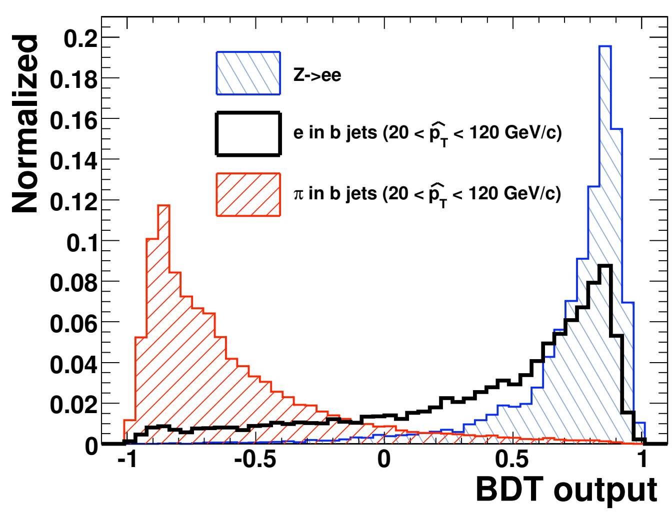

Figure 9: Output of the Boosted Decision Tree (BDT) used in the preselection of electrons with tracker driven only seed: (solid thick line) response for electrons in b-jets, (filled histogram) electrons from Z→ee decays, (filled histogram) pions in b-jets.

Figure 10 shows the electron reconstruction efficiency after the preselection as a function of generated electron η^e and p_T^e for electrons with uniform η^e and p_T^e distributions with $p_T^e > 2$ GeV$/c$. The reconstructed electrons are required to match generated electrons in charge and in direction within a cone of size $\Delta R = 0.05$. The efficiency is above $\simeq 90\%$ over the entire η range apart from the crack regions $|\eta| \simeq 1.5$ and $\eta \simeq 0$. The reconstruction efficiency rises steeply to reach $\simeq 90\%$ for $p_T^e \simeq 10$GeV$/c$ and then more slowly reaching a plateau of $\simeq 95\%$ for $p_T^e = 30$ GeV$/c$. The reconstruction efficiency after preselection for non-isolated electrons is presented in Fig. 11 for electrons and pions with $p_T > 2$ GeV$/c$ as a function of η and p_T on a sample of electrons from b-jets with p_T^{hat} within 20-120 GeV$/c$. Overall, an efficiency of 70% for electrons and 3.2% for pions is obtained.

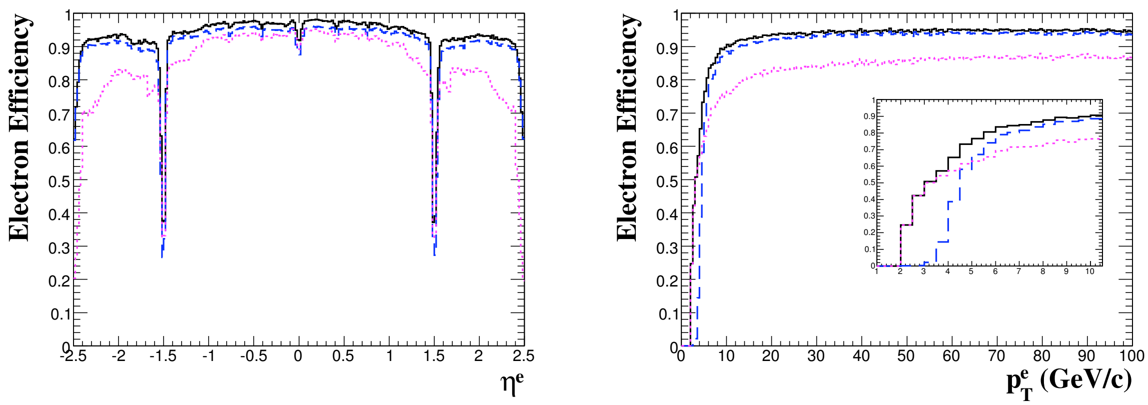

(a) (b)

Figure 10: Electron efficiency after preselection (solid line) as a function of (a) generated electron η^e and (b) generated electron p_T^e for a sample of di-electrons events with uniform distibution in η^e and p_T^e and with $p_T^e > 2$ GeV$/c$. The individual contributions from ECAL seeded electrons (dashed line) and from tracker seeded electrons (dotted line) are also shown, as well as a zoom of the region $p_T^e < 10.5$ GeV$/c$.

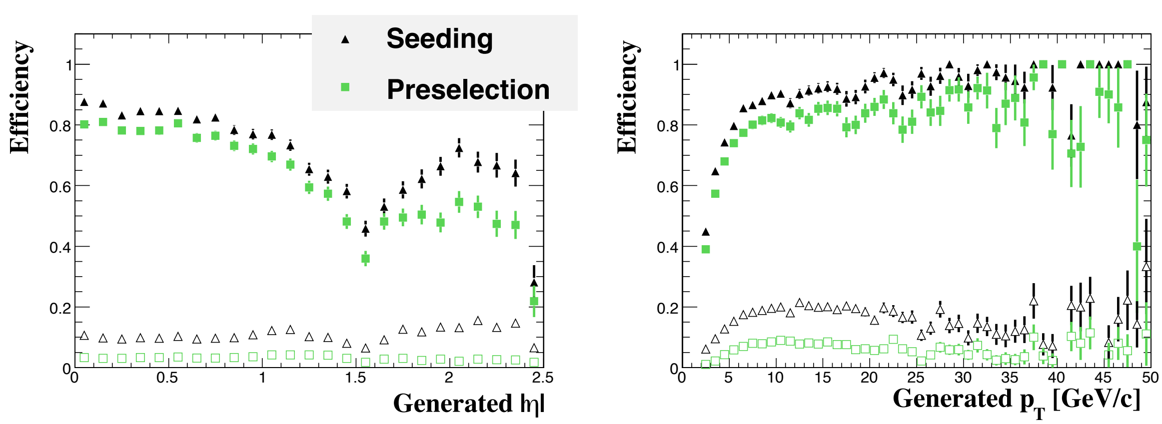

(a) (b)

Figure 11: Preselection performance for non-isolated electrons from a sample of b-jets with p_T^{hat} within 20-120 GeV$/c$ as a function of (a) generated $|\eta^e|$ and (b) generated p_T^e. Efficiencies are shown for electrons (plain markers) and pions (empty markers) as well as for the individual contributions from seeding (squares) and preselection (triangles) steps.

The background for isolated electrons is constituted by jets faking electrons due to $\pi^\pm$ interacting in the ECAL and $\pi^0/\pi^\pm$ overlap as well as real electrons from heavy flavors decays or from conversions from photons from π^0 decays. The fake rate defined as the fraction of reconstructed jets matched with a reconstructed electron is presented on Fig. 12 as a function of the reconstructed jet η. Jets are reconstructed using the iterative cone algorithm. A cone size of 0.3 is used to match reconstructed jets with reconstructed electrons.

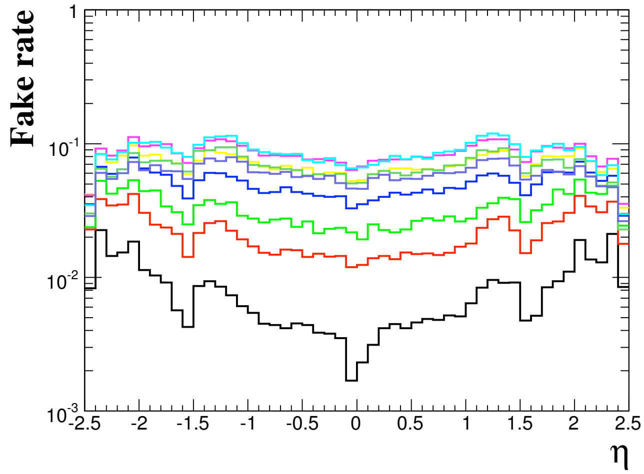

Figure 12: The fraction of reconstructed jets matched with a reconstructed electron as a function of the reconstructed jet η. Reconstructed electrons are required to have p_T^e >5 GeV/c. Events are from QCD dijet samples in different p_T^{hat} bins ranging from 0 to 300 GeV/c.

5 Removal of Conversions from Bremsstrahlung Photons

Once preselected, a further selection step is applied to remove ambiguous electron candidates that arise from the reconstruction of conversion legs from photon(s) radiated by primary electrons. With a $\simeq 2X0$ peak integrated amount of material budget in the tracker, electrons undergo in many cases several bremsstrahlung emissions eventually followed by conversions. Moreover, in the case of an emitted photon taking more than half of the original electron p_T, the predicted position in the next layer is closer to the photon than to the electron after emission. If the photon converts, the hits from its conversion legs will likely be efficiently found by the electron track reconstruction algorithm. On a sample of back-to-back di-electron events at fixed $p_T^e = 35$ GeV/c, $\simeq 14\%$ of the events have more than 2 reconstructed GSF tracks.

In such bremsstrahlung conversion patterns, the reconstruction often leads to electron candidates constituted by closeby tracks associated to the same or closeby superclusters, hereafter defined as ambiguous candidates. The removal of ambiguous candidates is particularly needed for electrons with tracker driven seeds as this seeding algorithm doesn't require the first hit to be close to the nominal interaction point and can therefore easily reconstruct secondary tracks.

The removal of ambiguous electron candidates relies upon the identification of the reconstructed candidate corresponding to the primary electron. The ambiguity solving algorithm firstly identifies electron candidates having superclusters "in common". For candidates with seed only found by the tracker driven algorithm, the supercluster is built following the tracker driven approach and is therefore always different from the supercluster of a candidate with seed found by the ECAL driven approach. Therefore, two superclusters are considered "in common" if a minimum energy is shared. Having identified candidates with common supercluster, the ambiguity resolution algorithm classifies the corresponding electrons according to their innermost track hit position. If two ambiguous electron candidates have their first hit on different layers, the candidate having the innermost first hit is kept. If both candidates have their first hit on the same tracker layer, and if both tracks have an ECAL driven seed, the candidate with best E/p ratio is kept. If both candidates have tracks with first hits in the same layer and one has a tracker driven seed, the following additional cleaning is applied: candidates constituted by a track having a different charge estimate at the innermost and outermost position or sharing at least 2 hits and more than 50% of tracker modules with the track of another candidate are removed.

Finally, cases where two electron candidates are constituted from different superclusters having seeded the same track are resolved by keeping the best E/p combination.

After this procedure is applied, the residual contamination from conversion legs can be estimated from the lower part of the invariant mass spectrum of reconstructed pairs on a sample of Z→ee decays: less than 0.5% of electron pairs are found to have an invariant mass smaller than 2.5 GeV/c^2 and in excess to the expectation from simple extrapolation of the spectrum from high masses to the region m$_{ee} \simeq 0$.

6 Electron Charge Determination

Electron charge identification suffers from the conversion of radiated photons and more generally from the showering of primary electrons in particular when this happens early in the detector. To overcome the lack of coverage of the pixel detectors, TEC layers are used in the very forward region ($|\eta| \gtrsim 2$) to seed electron tracks, significantly increasing the probability to pick up in the track reconstruction hits from conversions of bremsstrahlung photons or from more complicated showering of the primary electron before reaching these layers. The charge identification performance as obtained from the curvature of the GSF electron track is shown on Fig. 13 as a function of η^e and p_T^e from a sample of back-to-back electrons with uniform p_T^e and η^e distributions. The charge mis-identification (or charge mis-ID) nearly linearly increases in the region $1.1 < |\eta^e| < 2.5$, following the distribution of the material budget of the pixel detectors which reaches $\simeq 0.6X_0$ at $|\eta^e| = 2.5$. The charge mis-ID from the GSF track charge also increases as a function of p_T^e and amounts to $\simeq 3\%$ at the Z peak.

The charge determination can be improved by combining several charge estimates in a majority method that takes the value from the two out of three estimates that are in agreement. The three charge estimates used are: the GSF track charge, the general track charge and the supercluster charge. Other charge estimates such as the GSF track curvature at the outermost position have been studied and shown to be less performant. The general track charge is obtained by matching the GSF track with general tracks as reconstructed for pions and muons, asking for at least one hit shared in the innermost part (pixels). The supercluster charge is obtained by computing the sign of the ϕ difference between the vector joining the beam spot and the supercluster position and the one joining the beam spot and the first hit of the electron track. The result is shown on Fig. 13. One can see a significant improvement in the charge determination, by a factor ~ 2 or more over the entire p_T^e range. At the Z peak ($p_T^e \simeq 40$ GeV/c), the resulting charge mis-ID from the majority method is at the level of 1.2%.

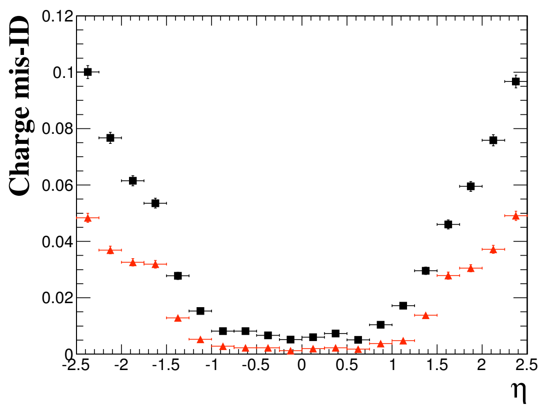

(a)

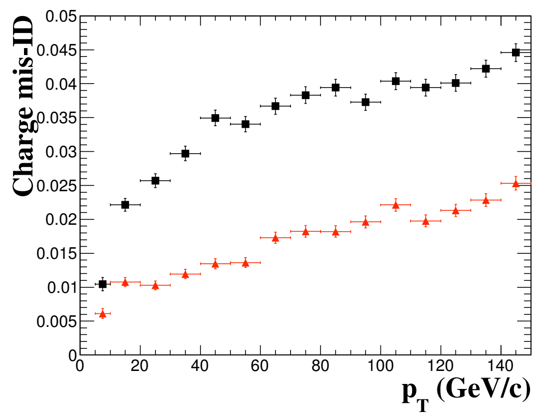

(b)

Figure 13: Electron charge mis-ID as obtained from the GSF track charge (squares, black) and from the majority method (triangles, red) as a function of (a) generated electron η^e and (b) generated electron p_T^e. The sample used is made of back-to-back electrons with uniform p_T^e and η^e distributions.

Selection methods can be used to further improve the charge identification. Here, a higher correctness in the charge determination is obtained to the price of a small efficiency loss, contrary to the above results with the majority method obtained without any loss of reconstructed electrons. The charge determination improvement is obtained by choosing two charge estimates and requiring that they give the same value, taking this value as the electron charge, or, to even further increase the correctness of the charge determination, by requiring that all three estimates agree. Figure 14 presents the charge mis-ID of the different selection methods obtained by requiring the agreement of two or all three estimates as a function of the generated electron p_T^e. The corresponding efficiency loss is also presented. Depending on the required degree of purity of the charge determination, one can choose a selection method to the price of a more or less severe loss in efficiency. A charge mis-ID rate below 0.4% can for instance be obtained over the entire p_T^e range for an efficiency loss ranging from 2 to 10%.

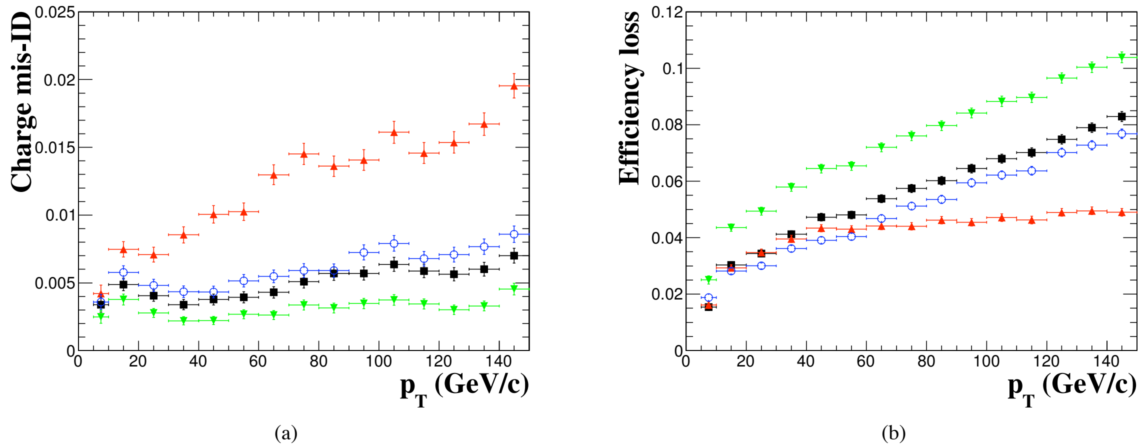

Figure 14: Electron charge ID performance as a function of generated p_T^e for the different selection methods: (a) charge mis-ID (b) corresponding selection efficiency. The selection methods are obtained by requiring the agreement of the charge estimates from: the GSF track and the associated general track (upward triangles, red), the general track and the supercluster position (circles, blue), the GSF track and the supercluster position (squares, black) and the GSF track, the general track and the supercluster position (downward triangles, green). The sample used is made of back-to-back electrons with uniform p_T^e and η^e distributions.

7 Momentum Determination and Electron Classes

The electron momentum magnitude is obtained from the combination of the ECAL and the tracker measurements, so to take advantage of the track momentum estimate in particular in the low energy region and/or in the ECAL crack regions. Starting from the energy as obtained from the supercluster after ECAL level corrections (from hereafter labelled E), the momentum magnitude can be further refined by splitting electrons into different classes and performing class dependant corrections. Following [4], the electron classification is based on the observed number of clusters inside the supercluster in the ECAL and on the measured bremsstrahlung fraction by the tracker. The classification has been further refined and the electron classes are defined as follows:

- "golden", or low breming electrons with a reconstructed track well matching the supercluster:
  - a supercluster formed by a single cluster (i.e. without observed bremsstrahlung sub-cluster),
  - a ratio $E/p > 0.9$,
  - a measured brem fraction $f_{brem} < 0.5$;
- "big brem", or electrons with high bremsstrahlung fraction but no evidence of energy loss effects:
  - a supercluster formed by a single cluster,
  - a ratio $E/p > 0.9$,
  - a measured bremsstrahlung fraction $f_{brem} > 0.5$;
- "showering", or electrons with energy pattern highly affected by bremsstrahlung losses:
  - a supercluster formed by a single cluster not falling in the "golden" or "big brem" classes, or a supercluster formed by several sub-clusters.

In addition, "crack" electrons are defined as electrons whose supercluster's starting crystal is close to an η boundary between ECAL barrel modules, or close to an η boundary betwen the ECAL barrel and ECAL endcaps. The population of electrons in the different classes is shown in Fig. 15 as a function of the generated η for electrons with a uniform p_T^e distribution between 2 and 150 GeV/c. The shape of the distribution for the showering class clearly reflects the η distribution of the material thickness. The integrated fractions of reconstructed electrons in the different classes are as follows: 29.8% (golden), 12.2% (big brem), 53.3% (showering) and 4.7% (cracks).

Figure 16 presents the peak value of the distribution of ratio between the supercluster and the generated energy as a function of the supercluster pseudorapidity (as seen from (0,0,0)) and of the supercluster energy for electrons

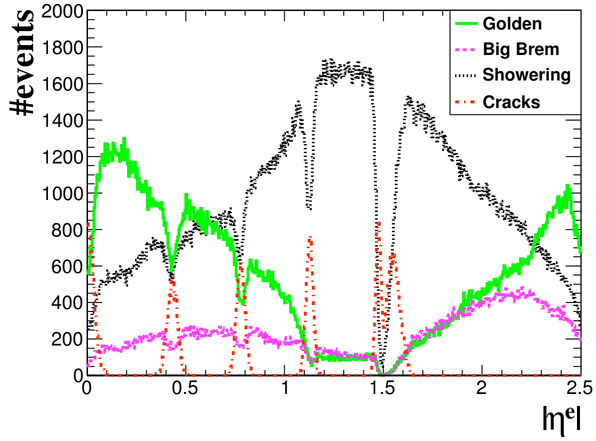

Figure 15: The electron population in the different classes as a function of the generated pseudorapidity for di-electrons with an initial transverse momentum uniformely distributed between 2 and 150 GeV/c.

from the golden, big brem and showering classes. The peak value is obtained by fitting the Gaussian part of the distribution in slices of pseudorapidity and energy.

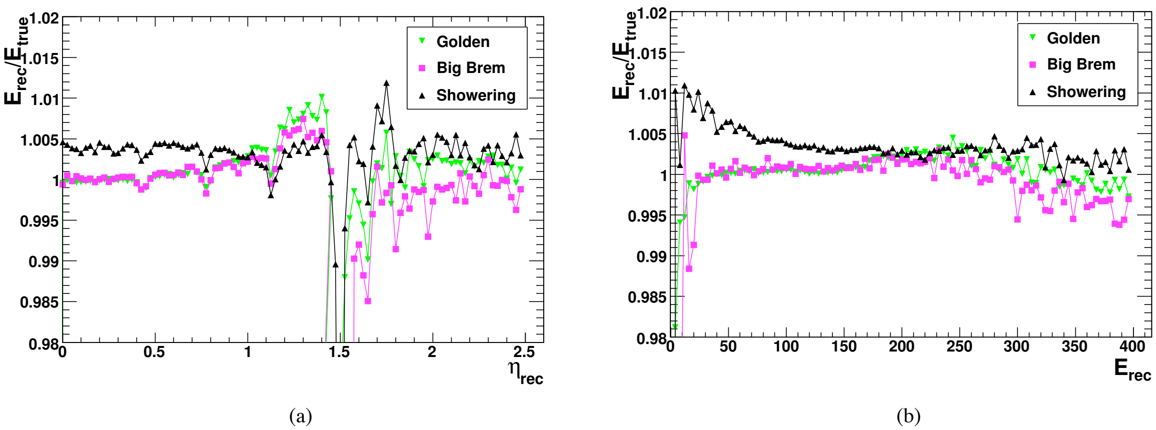

Figure 16: Fitted peak value of the reconstructed supercluster energy over the generated energy E/E^e for electrons from the golden (downward triangles, green), big brem (squares, magenta) and showering (upward triangles, black) classes as a function of (a) the reconstructed supercluster pseudorapidity η and (b) the reconstructed supercluster energy E.

Overall the energy scale is within $\pm$ 0.5% from the nominal value of 1, appart for showering electrons and energies up to $\simeq$ 50 GeV for which a significant overestimation from the supercluster corrected energy is observed. A slight offset of $\simeq 0.3\%$ is found for showering electrons over the entire η and energy range and could probably be corrected for at the supercluster level, and a residual trend in η is observed for golden electrons. However these effects are small and in what follows no further corrections are applied on the supercluster energy.

In order to combine the ECAL and tracker estimates, it is useful to analyze both measurement performance as a function of a variable sensitive to the amount of bremsstrahlung radiation. Figure 17 presents the ratios E/E^e and p/E^e as a function of E/p for the barrel case, where E stands for the supercluster corrected energy and p is the track momentum at the innermost track position using the mode estimate. A similar behaviour is found for the endcaps.

From these correlations one can identify three main regions:

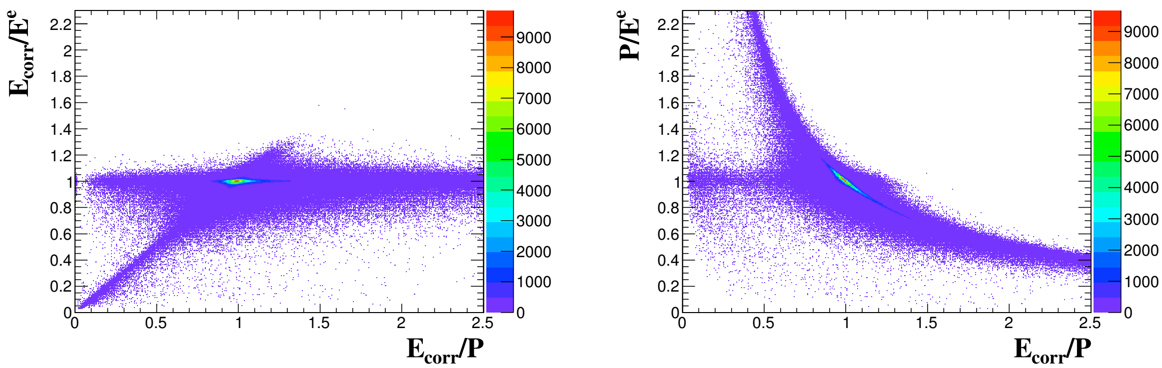

(a)

(b)

Figure 17: The momentum estimate from the ECAL and the tracker as a function of E/p for electrons in the ECAL barrel: (a) corrected supercluster energy normalized to the initial electron energy as a function of E/p; (b) reconstructed track momentum normalized to the initial electron energy as a function of E/p.

- cases with $E/p \sim 1$ where both the energy and momentum estimates are in good agreement with the generated value,
- cases with $E/p > 1$ where the tracker momentum measurement is always underestimated,
- cases with $E/p < 1$ where either the ECAL or the tracker measurement can be incorrect. Most of these cases correspond to showering electrons.

Following [4], the measurements are combined or only one measurement is used according to the above considerations on their respective sensitivity to bremsstrahlung induced effects. A weighted mean is used that involves the error determination on the supercluster energy and the error on the track momentum from the GSF fit. In addition to the use of supercluster provided errors, the algorithm has been updated with respect to [4] and the electron momentum magnitude is defined as the weighted mean of E and p when $|E/p - 1| < 2.5\sigma_{E/p}$ with weights computed as the normalized inverse of the variance of each measurement. In all the other cases, the ECAL measurement is used, except for the following cases for electrons in the ECAL barrel:

- the electron is golden and $E < 15$ GeV and $E/p < 1.15$
- the electron is showering and $E < 18$ GeV and $E/p < 1 - 2.5\sigma_{E/p}$
- the electron is in the crack class and $E < 60$ GeV and $E/p < 1 - 2.5\sigma_{E/p}$

or for, for electrons in the ECAL endcaps:

- the electron is golden and $E < 13$ GeV and $E/p < 1.15$

for which the tracker measurement is taken.

As can be expected, the tracker measurement is more used at low energies as well as in the regions where the precision of the ECAL measurement is poor. The performances of the combined electron momentum are illustrated in Fig. 18 which presents the normalized momentum effective RMS of the combined estimate as well as of the ECAL and tracker measurements alone for electrons in the ECAL barrel. Electrons are from a sample of di-electron events with uniformly distributed transverse momentum between 2 and 150 GeV/c. The precision is clearly improved by using the combined estimate with respect to the ECAL only measurement for energies below $\simeq$ 25-30 GeV. The normalized effective transverse momentum resolution for electrons in the ECAL barrel and electrons in the ECAL endcaps is also shown in Fig. 18.

The normalized effective RMS of the ECAL estimate and of the combined estimate are presented for the different classes in Fig. 19 as a function of the generated electron energy for electrons in the ECAL barrel. Golden electrons

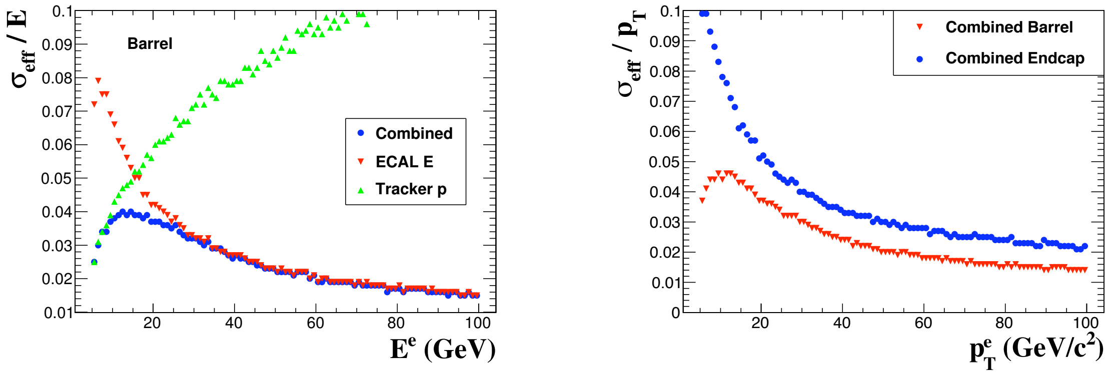

(a) (b)

Figure 18: Performances of the combined momentum estimate: (a) effective momentum resolution for the ECAL, the tracker and the combined momentum estimates as a function of the electron generated energy for electrons in the ECAL barrel and (b) effective transverse momentum resolution for electrons in the ECAL barrel and electrons in the ECAL endcaps. Electrons are from a sample of di-electron events with uniformly distributed transverse momentum between 2 and 150 GeV/c.

show a significantly better resolution than the average electron, with an asymptotic effective RMS of $\sim$1%. A significant degradation of the resolution is visible for showering electrons as well as for electrons from the crack class.

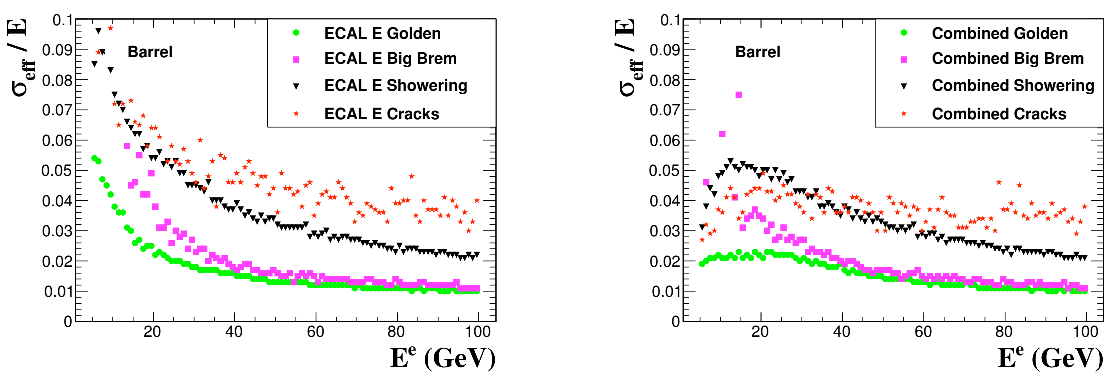

(a) (b)

Figure 19: Effective resolution for the different electron classes as a function of the electron generated energy for electrons in the ECAL barrel (a) from the ECAL measurement only and (b) after the combination with the tracker measurement. Electrons are from a sample of di-electron events with uniformly distributed transverse momentum between 2 and 150 GeV/c.

Figure 20 presents the distribution of the transverse momentum magnitude normalised to the generated transverse momentum as obtained for electrons from Z$\rightarrow$ee decays, as well as residual distributions of the momentum η and ϕ directions. The electron momentum direction is taken from the GSF track angle at the point of closest approach to the beam spot, using the mode estimate.

Finally, when the electron has been found by the tracker driven method and not by the ECAL driven method, the energy built from the tracker driven reconstruction of superclusters is used to construct the 4-momentum. In these cases, the electron momentum is simply constructed from the track direction and the supercluster energy.

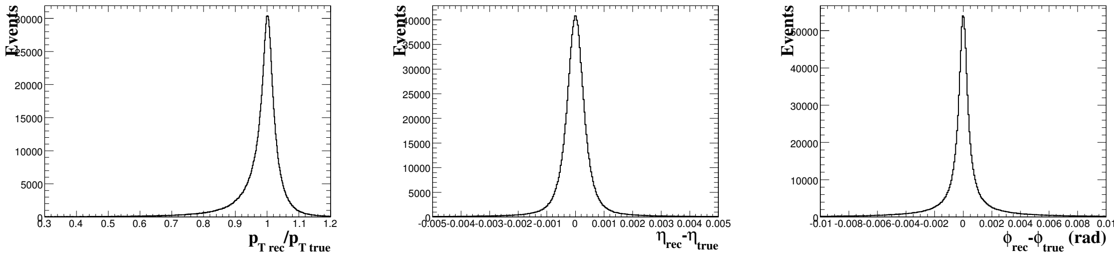

(a) (b) (c)

Figure 20: Final electron momentum parameters residual distributions for electrons from Z→ee decays: (a) transverse momentum magnitude (b) momentum η direction and (c) momentum ϕ direction.

8 Low p_T Electrons

At very low p_T^e, the clusters corresponding to electrons and radiated photons can be very far away due to the bending in the magnetic field and fall outside the ϕ window used in the reconstruction of superclusters. The current extension corresponds to a cut at $\simeq 0.5$ on the fraction $\alpha = p_T^\gamma / p_T^e$ of momentum taken away by the photon for an initial electron momentum of $p_T^e = 5$ GeV$/c$ and considering the worst case of a photon emitted at $r_\gamma \simeq 0$. Using wider ϕ window would lead to an increased contamination from close-by particles or noise. Therefore, in the ECAL driven strategy, all the ϕ windows used throughout the reconstruction have been optimised to efficiently reconstruct electrons down to $p_T^e = 5$ GeV$/c$ and, consistently, a threshold at 4 GeV in the supercluster E_T is used in the seeding.

To overcome this limitation and also for the purpose of reconstructing electrons inside jets, a different strategy has been developed for the bremsstrahlung recovery in the context of the particle flow reconstruction [17, 18]. The track/photon-cluster association criteria used in this procedure is purely geometrical. The position of the particle is extrapolated into the ECAL, at a depth corresponding to the expected maximum of the shower. The track/photon is matched with a cluster if the extrapolated position lies within the boundaries of one crystal constituting the cluster. The boundaries of the cells are appropriately enlarged to account for the presence of gaps between calorimeter cells, cracks between calorimeter modules and for the uncertainty of the position of the shower maximum. Based on the GSF track, a tangent is extrapolated at each track measurement toward the ECAL to identify a possible corresponding bremsstrahlung photon. As to minimize the contribution of the charged hadrons, the ECAL clusters matched with a Kalman Filter track, with the previously described criteria, are excluded from this procedure. Finally, the GSF is extrapolated from its outermost position into the ECAL, and the corresponding cluster is identified as the "electron" cluster. This approach allows the contributions of additional particle clusters to be limited.

The performance of the bremsstrahlung recovery for low p_T electrons are illustrated on Fig. 21 (a) which presents the distributions of the energy associated with the electron cluster as well as the distribution of the energy after the bremsstrahlung recovery procedure, normalised to the generated energy. Events are constituted from back-to-back electrons with a uniform p_T distribution between 2-10 GeV$/c$. To illustrate the maximum recoverable energy, the sum of the particle flow cluster energy in a $\Delta\eta = 0.2 \times \Delta\phi = 1.5$ window around the electron direction, normalised to the generated electron energy is also presented. It should be noted that the obtained energy measurement is not yet calibrated. Work is ongoing to apply a similar correction procedure as the one used for the hybrid and the multi5x5 superclustering algorithms.

One can see that with the tangent method, an efficient recovery of the bremsstrahlung clusters at low p_T^e is obtained. A source of limitation comes from subsequent conversion of radiated photons, especially in the region where the material budget is the highest ($|\eta| \simeq 1.5$). A method to identify conversions in this context is under work. In addition, as visible on Fig. 21 (b), where the recovered energy for non-isolated electrons in b jets and isolated electrons with the same kinematics as in b-jets is compared, this procedure has little sensitivity on the non-isolation.

9 Startup

The algorithms used in the electron reconstruction as well as the loose selection performed to reject part of the QCD background will have to be controled with the first data. Many data driven techniques can be used to monitor

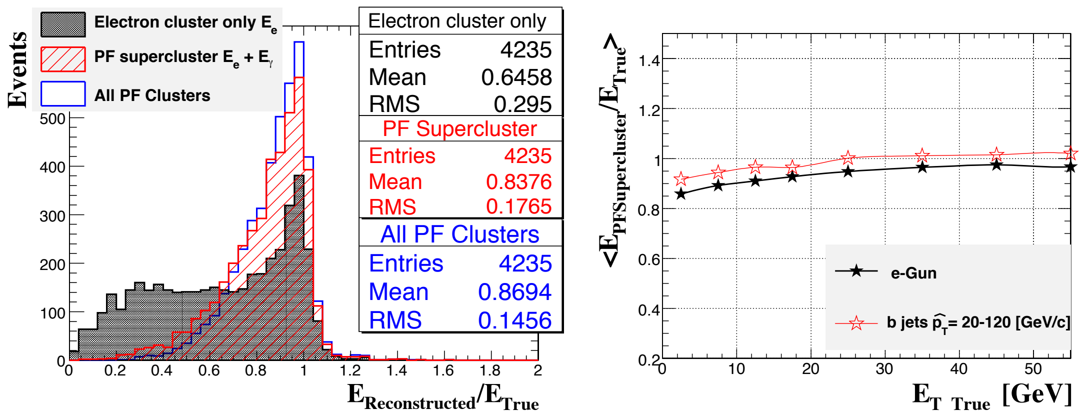

(a) (b)

Figure 21: Performance of the bremsstrahlung recovery procedure: (a) normalised distributions of the energy associated to the "electron" cluster, of the total energy associated with the electron track, and of the maximum recoverable energy (see text) for electrons with p_T^e between 2 and 10 GeV/c, and (b) recovered energy normalised by the true energy in the isolated and non-isolated case.

the reconstruction. The tag and probe technique in particular allows to constitute samples of isolated electrons of high purity from Z→ee decays, taking advantage of the mass constraint. It will be used to control the distributions of selection observables that enter the reconstruction as well as for the measurement of reconstruction efficiencies [19, 20, 21] and for the final determination of the energy scale [22]. At very low luminosity, the usage of low mass resonances can also be considered.

The beam spot position is used in the seeding of electron tracks and in particular in the ecal driven seeding aiming at seeding tracks from primary electrons. The seed matching algorithm makes use of the beam spot position to build the helices that drive the search of the first and second hits in the innermost part of the tracker. A mis-measurement of the beam spot transverse position can therefore lead to some efficiency loss. A sensitivity study has been recently performed using a sample of electrons from Z→ee where the beam spot position was artificially offset from the generated vetex position from 100 μm up to 1 cm along the y axis. Figure 22 shows the effect on reconstruction efficiency of a mis-measured position of the beam spot. As can be seen, overall the efficiency is quite stable and only drops for offset values of order or above 5 mm. As can be expected, the ecal driven seeding with its seed matching algorithm is more sensitive and starts showing some efficiency loss for values $\simeq$ 0.5 mm, corresponding to the window size in ϕ of the second layer ($\pm$ 4 mrad) at the 7 cm distance from the interaction point. This is expected to be well above the transverse beam size, even for the initial run at 1.1 TeV where it is already considerably larger than for the nominal parameters. The efficiency as a function of the generated electrons ϕ direction is also shown on Fig. 22 for a y offset of 1 mm. One can notice caracteristic "holes" in the efficiency pattern in the direction perpendicular to the beam spot offset.

The effect is similar to a mis-alignment of the pixel layers used in the ecal driven seeding. Initial mis-alignement scenario was studied during CSA08 [23], and $\simeq$ 10% loss in efficiency was found for a second ϕ window of ± 2 mrad with a particular striking ϕ efficiency pattern caracteristic of misaligned modules at specific ϕ positions. The efficiency loss was shown to be fully recovered by using a larger ϕ window as currently used in the reconstruction, as well as by applying the first alignment with data corresponding to 10 pb^{-1} of integrated luminosity. The redundancy of using 2 out of 3 layers to match the seed was in addition found to protect the efficiency that would in this configuration have dropped to nearly 0 if only two layers were used.

The efficiency and reliability of the pattern recognition as well as the robustness of the GSF fit will be based on the comparison of MC with data and the extraction and optimisation of the material constants from the first data. It will in a first step be validated through the comparison with the standard tracking as used for muons and pions. In particular the comparison of the hit collection for isolated mips will provide a test of the basic functionalities of the electron pattern recognition and of its sensitivity to detector noise and rechit properties.

The electron observables and therefore the loose selection performed in the electron reconstruction are in general sensitive to the amount of material budget in the tracker detector. Several observables have been used in past experiments to evaluate the material budget: the carateristic right hand side tail of the measured E/p distribution

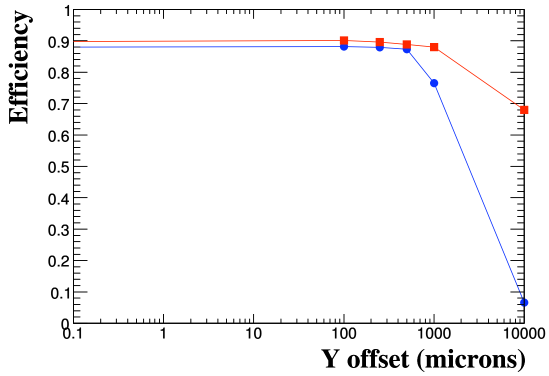

(a)

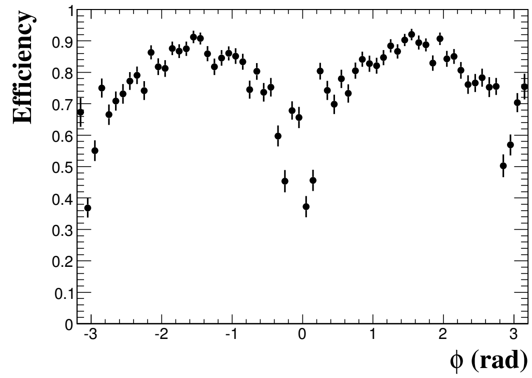

(b)

Figure 22: Effect of a mis-measurement of the beam spot on the reconstruction efficiency: (a) overall efficiency as a function of a bean spot offset along the y axis; the contribution of ecal driven electrons is shown separately (b) ϕ efficiency for ecal driven electrons and for a beam spot offset of 1 mm.

can for instance be used to adjust the material description used in simulation and in the reconstruction. Moreover, the difference between the GSF estimates at the outermost and innermost track positions is sensitive to the total amount of material budget and has been proposed to estimate the amount of material and associated systematics on the electron selection [5]. Such method can be extended to the evaluation of the material budget at each individual layers.

10 Conclusions

A refined strategy for electron reconstruction has been presented, based on a detailed Monte carlo simulation of the CMS detector.

The ECAL driven seeding algorithm, based on the matching of tracker seeds with reconstructed superclusters provides an efficient filtering of the background from jets faking electrons. It is complemented by a tracker driven seeding, which allows to further improve the efficiency at low p_T^e and in the ECAL crack regions. Overall, the seeding efficiency for isolated electrons is $\simeq$ 95% for $p_T^e = 10$ GeV/c and close to 100% for $p_T^e = 100$ GeV/c. A dedicated tracking and fitting is used for electrons to better cope with the large amount of radiative energy loss in the tracker material. The trajectory building strategy allows for an efficient collection of hits up to the ECAL despite important change of curvature undergone by electrons emitting bremsstrahlung photons. The mode estimates are used in the evalutation of the track momentum parameters. A loose preselection is applied on electron candidates which allows to keep a very high efficiency while rejecting a significant part of the background. In order to efficiently reconstruct non-isolated electrons a multivariate analysis is used to preselect electrons where only a tracker driven seed has been found. The reconstruction efficiency on isolated electrons is $\simeq 90\%$ for $p_T^e = 15$ GeV/c and $\simeq 95\%$ for $p_T^e = 100$ GeV/c. Electrons from reconstructed conversion legs are cleaned by resolving cases where several tracks are associated to the same supercluster. The electron charge is obtained by comparing several charge estimates in a majority method, allowing for a factor $\sim$2 improvement in the charge assignment over the p_T^e range 5-150 GeV/c. Selection methods are proposed to further improve the charge determination to the price of a small efficiency loss. A charge mis-ID below 0.4% can be obtained over the entire p_T^e range for an efficiency loss ranging from 2-10%. The final electron momentum is based on the combination of the ECAL and tracker measurements. ECAL superclusters errors as well as errors from the track fit are used in a weighted mean when the two measurements are in agreement. In the other cases, either the E measurement or the p measurement is used, depending on electron classes. An effective resolution of $\simeq 1\%$ is obtained for golden electrons of $\mathrm{E}^e = 100$ GeV in the ECAL barrel. The electron reconstruction based on the ECAL driven seeding is complemented by a technique more appropriate for the reconstruction of low p_T^e and non-isolated electrons. The technique makes use of a more sophisticated bremsstrahlung recovery using tangents at each measurement position of the electron trajectory in order to identify possible bremsstrahlung clusters in the ECAL.

Data driven techniques will be used for the control of key reconstruction distributions as well as in-situ measurement of reconstruction efficiencies. Different scenarii have been studied to assess the sensitivity of the reconstruction algorithms and selection cuts to initial conditions such as a limited knowledge of the beam spot position and/or an initial mis-alignement of the tracker layers, or a limited knowledge of the amount of material budget. The described algorithms make use of robust variables and a selection with sufficient safety margin in view of the initial CMS data taking. It is expected that, once the detector will be better known, the choice of selection variables and of the efficiency/fake rate working point will be further refined.

11 Acknowledgments

We wish to thank the CMS e/gamma working group for the support.

References

[1] CMS Collaboration, "The Trigger and Data Acquisition Project, Volume II", CERN/LHCC 2002-26 (2002).

[2] E. Meschi *et al.*, "Electron reconstruction in the CMS Electromagnetic Calorimeter", CMS Note 2001/034.

[3] CMS Collaboration, "CMS Physics Technical Design Report, Volume I: Detector Performance and Software", CERN-LHCC-2006-001, CMS-TDR-8.1 (2006).

[4] S. Baffioni *et al.*, "Electron reconstruction in CMS", Eur. Phys. J. C **49** (2007) 1099.

[5] S. Baffioni *et al.*, "Discovery Potential for the SM Higgs Boson in the $\mathrm{H}\rightarrow\mathrm{ZZ}^{(*)}\rightarrow\mathrm{e}^+\mathrm{e}^-\mathrm{e}^+\mathrm{e}^-$ Decay Channel", J. Phys. G **34** (2007) N23.

[6] W. Adam *et al.*, "Reconstruction of electrons with the Gaussian-sum filter in the CMS tracker at the LHC", J. Phys. G: Nucl. Part. Phys. 31 N9-N20 (2005).

[7] C. Charlot *et al.*, "Reconstruction of Electron Tracks Using Gaussian Sum Filter in CMS", CMS AN 2005/011.

[8] S. Baffioni *et al.*, "Electron selection and identification in CMS", CMS AN 2005/065.

[9] J. Branson *et al.*, "A cut based method for electron identification in CMS", CMS AN 2008/082.

[10] E. Di Marco *et al.*, "Electron identification in the CMS experiment based on a likelihood algorithm", CMS AN 2008/110.

[11] CMS Collaboration, "Electron Identification in CMS", CMS AN 2009/178 (in preparation).

[12] S. Baffioni *et al.*, "Electron reconstruction: e Classes, E scale Corrections and E-p combination", CMS AN 2005/062.

[13] M. Pioppi, "Electron Pre-identification in the Particle Flow framework", CMS AN 2008/032.

[14] K. Lassila-Perini, "Jet Rejection with Matching ECAL Clusters to Pixel Hits", CMS Note 2001/021.

[15] A. Martelli, "Optimisation of electron reconstruction in the CMS experiment", Diploma Thesis, U. Milano Bicocca (2008) 93pp.

[16] W. Adam *et al.*, "Track reconstruction in CMS tracker", CMS Note 2006/41 (feb. 2006).

[17] The CMS Collaboration, "Particle-Flow Event reconstruction in CMS and Performance for Jets, Taus, and E_T^{miss} ", CMS PAS PFT-09/001.

[18] The CMS Collaboration, "Electron reconstruction within the Particle Flow Algorithm", CMS PAS PFT-09/006 (in preparation).

[19] N. Adam *et al.*, "Generic Tag and Probe Tool for Measuring Efficiency at CMS with Early Data", CMS AN-2009/111.

[20] CMS Collaboration, "Measuring Electron Efficiencies at CMS with Early Data", CMS PAS EGM-07-001 (dec. 2007).

[21] G. Daskalakis *et al.*, "Measuring Electron Efficiencies at CMS with Early Data", CMS AN 2007/019 (nov. 2007).

[22] P. Meridiani *et al.*, "Use of $Z \rightarrow e^+e^-$ events for ECAL calibration", CMS Note 2006-039 (jan. 2006) 18pp.

[23] CMS collaboration, "The 2008 CMS Computing, Software and Analysis Challenge", CMS IN 2008/044 (nov. 2008).